Fracture of Elastomeric Materials by Crosslink Failure

Fracture of Elastomeric Materials by Crosslink Failure

Yunwei Mao
Department of Mechanical Engineering,
Massachusetts Institute of Technology,
Cambridge, MA 02139

Lallit Anand[1]
Department of Mechanical Engineering,
Massachusetts Institute of Technology,
Cambridge, MA 02139
e-mail: anand@mit.edu

If an elastomeric material is subjected to sufficiently large deformations, it eventually fractures. There are two typical micromechanisms of failure in such materials: chain scission and crosslink failure. The chain scission failure mode is mainly observed in polymers with strong covalent crosslinks, while the crosslink failure mode is observed in polymers with weak crosslinks. In two recent papers, we have proposed a theory for progressive damage and rupture of polymers with strong covalent crosslinks. In this paper, we extend our previous framework and formulate a theory for modeling failure of elastomeric materials with weak crosslinks. We first introduce a model for the deformation of a single chain with weak crosslinks at each of its two ends using statistical mechanics arguments, and then upscale the model from a single chain to the continuum level for a polymer network. Finally, we introduce a damage variable to describe the progressive damage and failure of polymer networks. A central feature of our theory is the recognition that the free energy of elastomers is not entirely entropic in nature; there is also an energetic contribution from the deformation of the backbone bonds in a chain and/or the crosslinks. For polymers with weak crosslinks, this energetic contribution is mainly from the deformation of the crosslinks. It is this energetic part of the free energy which is the driving force for progressive damage and fracture of elastomeric materials. Moreover, we show that for elastomeric materials in which fracture occurs by crosslink stretching and scission, the classical Lake–Thomas scaling—that the toughness G_c of an elastomeric material is proportional to $1/\sqrt{G_0}$, with $G_0 = Nk_B\vartheta$ the ground-state shear modulus of the material—does not hold. A new scaling is proposed, and some important consequences of this scaling are remarked upon. [DOI: 10.1115/1.4040100]

Keywords: polymers, damage, rupture, phase-field theory, gradient-damage theory

1 Introduction

Soft elastomeric materials are widely used in applications such as carriers for drug delivery, scaffolds for tissue engineering, soft actuators, and smart optical systems, and as packers for sealing oil-wells. One of the distinguishing features of these materials is that their deformation response is dominated by changes in entropy. Accordingly, most classical theories of rubber-like elasticity consider only changes in entropy and neglect any changes in internal energy. However, when subjected to sufficiently large deformations, these materials eventually fracture. While an accounting of changes in entropy can adequately describe the deformation of the material, such an accounting says nothing about the rupture because rupture is an *energetic* process at the microscale, emanating from the scission of molecular bonds in the polymer network. The molecular bonds will be ruptured only when the stored internal energy attains a certain critical value. Thus, while a neglect of an internal energy contribution simplifies the classical theories of rubber-like elasticity, it makes such theories incapable of dealing with rupture of soft materials.

There are two typical failure micromechanisms in soft materials: chain scission and crosslink failure. If the cross-linking chemical bonds in an elastomeric network are strong covalent bonds, then fracture is expected to occur by scission of the chains between the crosslinks, while if the chemical crosslinks are weak, then fracture is expected to occur because of the scission of the cross-linking bonds themselves.

Lake and Thomas [1] developed the first molecular theory for the fracture energy of elastomers with strong covalent crosslinks. They proposed that when any of the main bonds in a polymer chain breaks, then the total energy of each bond of the stretched chain is irreversibly lost. Therefore, the energy necessary to break a chain is proportional to the length of that chain, i.e., proportional to the number of backbone bonds, n, comprising the chain.[2] In an important paper, Akagi et al. [2] presented results from their investigations on the fracture behavior of tetra(polyethylene glycol) (Tetra-PEG) gels with precisely controlled network structures. These controlled network structures, with greatly suppressed heterogeneity, enabled these authors to validate the predictions of the Lake–Thomas model; also see Ref. [3].

In two recent papers [4,5], we presented a theory for fracture of an elastomeric solid in which, following the lead of Lake and Thomas [1], we focused our attention on networks with strong crosslinks, which fail by scission of the polymer chains between the crosslinks.[3] In that theory, a new field called the *effective bond stretch* λ_b was introduced to describe the stretchability and eventual failure of the Kuhn segments of polymer chains, but we neglected the stretchability of the crosslinks. However, in many synthetic polymers, the Kuhn segments are quite stiff and strong. Instead, it is the weak crosslinks in the network, which are stretched and eventually lead to failure.[4] *The purpose of the present paper is to present a theory in which failure occurs by crosslink failure rather than by chain scission.*

Much of the continuum-level theory developed in our previous papers is unchanged, but what is changed is that here we introduce

[1]Corresponding author.

Contributed by the Applied Mechanics Division of ASME for publication in the Journal of Applied Mechanics. Manuscript received January 26, 2018; final manuscript received April 27, 2018; published online June 4, 2018. Assoc. Editor: Thomas Siegmund.

[2]Actually proportional to $\sqrt{n}$; cf. Ref. [3] and also the Remark on page 12.

[3]Such as Tetra-PEG-gels of Ref. [2].

[4]For example, the 4-arm polyethylene glycol network with reversible metal-ligand crosslinks [6].

an *effective crosslink stretch* λ_c—rather than an effective bond stretch λ_b—as an internal variable of the theory. Also changed are the specialized constitutive equations for the internal energy and entropy of the network because the micromechanism of damage and failure is fundamentally different from what we had considered previously.

There is always a *damage process zone* in the vicinity of a crack. Thus, in order to model final fracture of the elastomer, we also introduce a damage variable $\mathrm{d}(\mathbf{X},t)\in[0,1]$. When $\mathrm{d}=1$ at some material point, then that point is fractured, and values of d between zero and one correspond to partially fractured material. For this reason, we develop a damage theory, which depends not only on d but also on its gradient $\nabla\mathrm{d}$, which represents a measure of the spatial inhomogeneity of the damage during the fracturing process. Hence, there is a material length scale, ℓ, in the vicinity of a crack over which the damage variable d varies between zero and one; ℓ therefore represents a measure of the "size of the damage process zone," Another reason for introducing a gradient-damage theory is to "regularize" the strain-softening behavior during the fracture process, and to avoid mesh dependency-related issues during finite element simulations—as is common in the recent phase-field theories of fracture [5,7–11]. Numerically, a gradient theory can ensure that the simulation results are mesh-independent, provided the mesh size is small enough; that is, typical element size h_e less than 0.2ℓ.

The plan of this paper is as follows: In Sec. 2, we summarize the essence of our continuum-level model. Since the structure of the continuum-level model is essentially unchanged from our recent paper [5], we simply reproduce the constitutive theory presented in Sec. 2 of Ref. [5] with the effective bond stretch λ_b replaced by an effective crosslink stretch λ_c.[5] In Sec. 3, we give the specialized constitutive equations, which allow for failure due to damage of crosslinks in the network. Moreover, we show that for elastomeric materials in which fracture occurs by crosslink stretching and scission, the Lake–Thomas scaling [1–3,12]—that is the toughness G_c is proportional to $1/\sqrt{G_0}$, with $G_0=Nk_b\vartheta$ the ground-state shear modulus of the material—does not hold. A new scaling is proposed, and some important consequences of this scaling are remarked upon. In Sec. 4, we study the capability of our theory and its numerical implementation in a finite element program to model *plane stress* fracture of (i) single-edge-notched specimens; (ii) an asymmetric double-edge-notched specimen; and (iii) fracture of a sheet specimen with multiple circular and elliptical holes. Finally, we summarize our main conclusions and make some final remarks in Sec. 5.

2 Summary of the Constitutive Theory, Governing Partial Differential Equations, and Boundary Conditions

At the continuum level, our theory is essentially that developed in our previous paper [5], but here we allow for an *effective crosslink stretch* λ_c, rather than an effective bond stretch λ_b, as an internal variable of the theory. Our theory relates the following basic fields:[6] $\mathbf{x}=\boldsymbol{\chi}(\mathbf{X},t)$, motion; $\mathbf{F}=\nabla\boldsymbol{\chi}$, $J=\det\mathbf{F}>0$, deformation gradient; $\bar{\mathbf{F}}=J^{-1/3}\mathbf{F}$, distortional part of $\mathbf{F}$; $\mathbf{C}=\mathbf{F}^{\top}\mathbf{F}$, right Cauchy–Green tensor; $\bar{\mathbf{C}}=\bar{\mathbf{F}}^{\top}\bar{\mathbf{F}}=J^{-2/3}\mathbf{C}$, distortional part of $\mathbf{C}$; $\mathbf{T}_{\mathrm{R}}$, $\mathbf{T}_{\mathrm{R}}\mathbf{F}^{\top}=\mathbf{F}\mathbf{T}_{\mathrm{R}}^{\top}$ Piola stress; $\mathbf{T}_{\mathrm{RR}}=\mathbf{F}^{-1}\mathbf{T}_{\mathrm{R}}$, second Piola stress; ψ_{R}, free energy density per unit reference volume; ε_{R}, internal energy density per unit reference volume; $\lambda_c>0$ effective crosslink stretch (an internal variable); $\mathrm{d}(\mathbf{X},t)\in[0,1]$, damage variable or phase-field with $\dot{\mathrm{d}}\geq 0$; ϖ scalar microstress conjugate to $\dot{\mathrm{d}}$; and $\boldsymbol{\xi}$ vector microstress conjugate to $\nabla\dot{\mathrm{d}}$.

2.1 Constitutive Equations

(1) Free energy
This is given by

$$\psi_{\mathrm{R}}=\hat{\psi}_{\mathrm{R}}(\boldsymbol{\Lambda}),\quad \text{with}\quad \boldsymbol{\Lambda}=\{\mathbf{C},\lambda_c,\mathrm{d},\nabla\mathrm{d}\} \tag{2.1}$$

(2) Second Piola stress and Piola stress
The second Piola stress and the Piola stress are given by

$$\mathbf{T}_{\mathrm{RR}}=2\,\frac{\partial\hat{\psi}_{\mathrm{R}}(\boldsymbol{\Lambda})}{\partial\mathbf{C}},\quad \mathbf{T}_{\mathrm{R}}=\mathbf{F}\mathbf{T}_{\mathrm{RR}} \tag{2.2}$$

(3) Implicit equation for the effective crosslink stretch
The thermodynamic requirement

$$\frac{\partial\hat{\psi}_{\mathrm{R}}(\boldsymbol{\Lambda})}{\partial\lambda_c}=0 \tag{2.3}$$

reflects the fact that the actual value of the effective crosslink stretch λ_c adopted by the material is the one that *minimizes* the free energy. This equation serves as an implicit equation to determine λ_c in terms of the other constitutive variables.[7]

(4) Microstresses ϖ and $\boldsymbol{\xi}$
The scalar microstress ϖ conjugate to the rate of change of the damage variable $\dot{\mathrm{d}}$ is given by

$$\varpi=\underbrace{\frac{\partial\hat{\psi}_{\mathrm{R}}(\boldsymbol{\Lambda})}{\partial\mathrm{d}}}_{\varpi_{\mathrm{en}}}+\underbrace{\alpha+\zeta\dot{\mathrm{d}}}_{\varpi_{\mathrm{diss}}} \tag{2.4}$$

with $\alpha=\hat{\alpha}(\boldsymbol{\Lambda})$ and $\zeta=\hat{\zeta}(\boldsymbol{\Lambda})$ positive-valued scalar functions.[8] Here, ϖ_{en} and ϖ_{diss} denote the energetic and dissipative parts of ϖ. The vector microstresses $\boldsymbol{\xi}$ conjugate to $\nabla\dot{\mathrm{d}}$ is given by

$$\boldsymbol{\xi}=\frac{\partial\hat{\psi}_{\mathrm{R}}(\boldsymbol{\Lambda})}{\partial\nabla\mathrm{d}} \tag{2.5}$$

and is taken to be purely energetic with no dissipative contribution.[9]

2.2 Governing Partial Differential Equations. The governing partial differential equations (PDE) consist of:

(1) Equation of motion

$$\mathrm{Div}\mathbf{T}_{\mathrm{R}}+\mathbf{b}_{0\mathrm{R}}=\rho_{\mathrm{R}}\ddot{\boldsymbol{\chi}} \tag{2.6}$$

[5]From the outset, we acknowledge that there is considerable overlap between this paper and our recent publication [5], and in addition to Sec. 2, there are several other phrases, paragraphs, and footnotes, which are (probably) the same as those in our previous paper, but are repeated here for a coherent narrative and completeness.

[6]Notation: We use standard notation of modern continuum mechanics [13]. Specifically: ∇ and Div denote the gradient and divergence with respect to the material point $\mathbf{X}$ in the reference configuration, and $\Delta=\mathrm{Div}\nabla$ denotes the referential Laplace operator; grad, div, and div grad denote these operators with respect to the point $\mathbf{x}=\boldsymbol{\chi}(\mathbf{X},t)$ in the deformed body; a superposed dot denotes the material time-derivative. Throughout, we write $\mathbf{F}^{-\top}=(\mathbf{F}^{-1})^{\top}=(\mathbf{F}^{\top})^{-1}$, etc. We write $\mathrm{tr}\mathbf{A}$, $\mathrm{sym}\mathbf{A}$, $\mathrm{skw}\mathbf{A}$, $\mathbf{A}_0$, and $\mathrm{sym}_0\mathbf{A}$ respectively, for the trace, symmetric, skew, deviatoric, and symmetric-deviatoric parts of a tensor $\mathbf{A}$. Also, the inner product of tensors $\mathbf{A}$ and $\mathbf{B}$ is denoted by $\mathbf{A}:\mathbf{B}$, and the magnitude of $\mathbf{A}$ by $|\mathbf{A}|=\sqrt{\mathbf{A}:\mathbf{A}}$.

[7]To limit the dynamics of failure by crosslink stretch, Eq. (2.3) may be modified by introducing a rate-dependent term of the form $\partial\hat{\psi}_{\mathrm{R}}(\boldsymbol{\Lambda})/\partial\lambda_c=-\kappa_c(\lambda_c)\dot{\lambda}_c$, as we did in Ref. [14].

[8]Detailed thermodynamic considerations result in the dissipation inequality (cf. Eq. (A. 48) in our recent paper [5]) $\mathcal{D}=\alpha\dot{\mathrm{d}}+\zeta\dot{\mathrm{d}}^2>0$ when $\dot{\mathrm{d}}>0$ The choice $\alpha\geq 0$ and $\zeta\geq 0$ ensures that this dissipation inequality is satisfied.

[9]Thermodynamics does not require that $\boldsymbol{\xi}_{\mathrm{diss}}=0$. However, it is a particular constitutive assumption that we make; cf. Eq. $(\mathrm{A}.46)_3$ of Ref. [5]. The assumption of a dissipative contribution ϖ_{diss} to the microstress ϖ conjugate to $\dot{\mathrm{d}}$, but no dissipative contribution $\boldsymbol{\xi}_{\mathrm{diss}}$ to the vector microstress $\boldsymbol{\xi}$ conjugate to $\nabla\dot{\mathrm{d}}$, is a typical choice which is made in recent gradient-damage/phase-field type theories for fracture, e.g., see Refs. [5,7–11]. In order to not depart too much from the recent literature, we have made a similar assumption in this paper as well.

where $\mathbf{b}_{0\mathrm{R}}$ is a noninertial body force, ρ_{R} is the referential mass density, $\ddot{\boldsymbol{\chi}}$ is the acceleration, and the Piola stress $\mathbf{T}_{\mathrm{R}}$ is given by $(2.2)_2$. In the numerical simulations presented later in the paper, we neglect all inertial effects.

(2) Microforce balance:
The microforces ϖ and $\boldsymbol{\xi}$ obey the balance

$$\mathrm{Div}\boldsymbol{\xi} - \varpi = 0 \tag{2.7}$$

This microforce balance, together with the thermodynamically consistent constitutive equations (2.4) and (2.5) for ϖ and $\boldsymbol{\xi}$, gives the following evolution equation for the damage variable d,[10]

$$\hat{\zeta}(\boldsymbol{\Lambda})\dot{\mathrm{d}} = -\frac{\partial\hat{\psi}_{\mathrm{R}}(\boldsymbol{\Lambda})}{\partial \mathrm{d}} + \mathrm{Div}\left(\frac{\partial\hat{\psi}_{\mathrm{R}}(\boldsymbol{\Lambda})}{\partial\nabla\mathrm{d}}\right) - \hat{\alpha}(\boldsymbol{\Lambda}) \tag{2.8}$$

Since ζ is positive-valued, the right-hand side of (2.8) must be positive for $\dot{\mathrm{d}}$ to be positive and the damage to increase monotonically.[11]

We also need boundary and initial conditions to complete the theory.

(1) Boundary conditions for the PDE governing the evolution of the motion $\boldsymbol{\chi}$:
Let $\mathcal{S}_{\boldsymbol{\chi}}$ and $\mathcal{S}_{\mathbf{t}_{\mathrm{R}}}$ be complementary subsurfaces of the boundary $\partial\mathrm{B}$ of the body B. Then for a time interval $t \in [0,T]$, we consider a pair of boundary conditions in which the motion is specified on $\mathcal{S}_{\boldsymbol{\chi}}$ and the surface traction on $\mathcal{S}_{\mathbf{t}_{\mathrm{R}}}$

$$\boldsymbol{\chi} = \breve{\boldsymbol{\chi}} \quad \text{on}\,\mathcal{S}_{\boldsymbol{\chi}} \times [0,T], \quad \text{and} \quad \mathbf{T}_{\mathrm{R}}\mathbf{n}_{\mathrm{R}} = \breve{\mathbf{t}}_{\mathrm{R}} \quad \text{on}\,\mathcal{S}_{\mathbf{t}_{\mathrm{R}}} \times [0,T] \tag{2.9}$$

In the boundary conditions above, $\breve{\boldsymbol{\chi}}$ and $\breve{\mathbf{t}}_{\mathrm{R}}$ are *prescribed* functions of $\mathbf{X}$ and t.

(2) Boundary conditions for the PDE governing the evolution of the damage variable d
The presence of microscopic stresses $\boldsymbol{\xi}$ results in an expenditure of power $\int_{\partial\mathrm{B}}(\boldsymbol{\xi}\cdot\mathbf{n}_{\mathrm{R}})\dot{\mathrm{d}}\,da_{\mathrm{R}}$ by the material in contact with the body, and this necessitates a consideration of boundary conditions on $\partial\mathrm{B}$ involving the microscopic tractions $\boldsymbol{\xi}\cdot\mathbf{n}_{\mathrm{R}}$ and the rate of change of the damage variable $\dot{\mathrm{d}}$. *We restrict attention to boundary conditions that result in a null expenditure of microscopic power in the sense that* $(\boldsymbol{\xi}\cdot\mathbf{n}_{\mathrm{R}})\dot{\mathrm{d}} = 0$. A simple set of boundary conditions which satisfies this requirement is

$$\dot{\mathrm{d}} = 0 \quad \text{on}\,\mathcal{S}_{\mathrm{d}} \times [0,T], \quad \text{and} \quad \boldsymbol{\xi}\cdot\mathbf{n}_{\mathrm{R}} = 0 \quad \text{on}\,\partial\mathrm{B}\backslash\mathcal{S}_{\mathrm{d}} \times [0,T] \tag{2.10}$$

with the microforce $\boldsymbol{\xi}$ given by (2.5).

The initial data are taken as

$$\boldsymbol{\chi}(\mathbf{X},0) = \mathbf{X}, \qquad \dot{\boldsymbol{\chi}}(\mathbf{X},0) = \mathbf{v}_0(\mathbf{X}), \quad \text{and} \quad \mathrm{d}(\mathbf{X},0) = 0 \quad \text{in} \quad \mathrm{B} \tag{2.11}$$

The coupled set of equations (2.6) and (2.8) together with Eqs. (2.9)–(2.11) yield an initial/boundary-value problem for the motion $\boldsymbol{\chi}(\mathbf{X},t)$, and the damage variable $\mathrm{d}(\mathbf{X},t)$.

3 Specialization of the Constitutive Equations

To build a predictive model, we wish to characterize the process of rupture in elastomeric materials with weak crosslinks in terms of the microscopic mechanics of molecular crosslink deformation and failure. However, traditional hyperelasticity models for elastomers neglect the energetics of crosslinks deformation. Accordingly, we formulate a hyperelastic constitutive model that accounts for the energetics of crosslink stretch, as well as the well-known entropic effects of polymer elasticity. In what follows, we begin by considering the process of deformation of a single chain, and then extend the single chain considerations to bulk polymer networks undergoing damage and eventual failure.

3.1 Deformation of a Single Chain. Consider a single chain with *n unstretchable* segments, each of initial length L_b. Let

- $r_0 = \sqrt{n}L_b$ denote the unstretched chain length determined from random-walk statistics, and
- let r denote the end-to-end distance of chain in a deformed configuration.

The classical freely jointed chain theory gives the free energy ψ of a single chain as [15] (as quoted in Ref. [16])

$$\psi = \hat{\psi}(r) = k_{\mathrm{B}}\vartheta n\left(\frac{r}{nL_b}\beta + \ln\left(\frac{\beta}{\sinh\beta}\right)\right) \quad \text{with} \quad \beta = \mathcal{L}^{-1}\left(\frac{r}{nL_b}\right) \tag{3.1}$$

where k_{B} is Boltzmann's constant, ϑ is the absolute temperature, and $\mathcal{L}^{-1}$ is the inverse of the Langevin function $\mathcal{L}(x) = \coth x - x^{-1}$.

In order to arrive to an expression for the free energy which accounts for cross-link deformation, we first consider the behavior of a single chain with a crosslink at each end, each of length L_c (see Fig. 1).

Generally, the overall deformation of the single polymer chain under load is due to three sources:

(i) the alignment of the Kuhn segments;
(ii) stretching of the Kuhn segments; and
(iii) stretching of the molecular bonds associated with crosslinks at each end.

We make the constitutive assumption that

- the Kuhn segments in the chain are much stiffer than the molecular bonds associated with the two crosslinks at each end so that the stretchability and the internal energy stored within the Kuhn segments is negligible.

To further simplify the physical picture, we assume that the configurational entropy stored within the molecular bonds associated with crosslinks are negligible, and that both the crosslink bonds are aligned with and follow the direction of the stretching force (cf. Fig. 1(*b*)).

The stretchable bonds associated with crosslinks may extend such that their deformed length is

$$l_c = \lambda_c L_c \tag{3.2}$$

where λ_c is a dimensionless stretch, which we refer to as the *cross-link stretch*. Then, with $\hat{\varepsilon}_{\mathrm{c}}(\lambda_{\mathrm{c}})$ denoting the internal energy associated with the stretching of the crosslinks, we take the free energy to be given by

$$\psi = \hat{\psi}(\tilde{r},\lambda_{\mathrm{c}}) = 2\hat{\varepsilon}_{\mathrm{c}}(\lambda_{\mathrm{c}}) + k_{\mathrm{B}}\vartheta n\left(\frac{\tilde{r}}{nL_b}\beta + \ln\left(\frac{\beta}{\sinh\beta}\right)\right) \quad \text{with} \quad \beta = \mathcal{L}^{-1}\left(\frac{\tilde{r}}{nL_b}\right) \tag{3.3}$$

and with

$$\tilde{r} = r - 2\,\lambda_c L_c \tag{3.4}$$

the net end-to-end distance of the part of the chain with rigid Kuhn segments. It is convenient to rewrite the free energy (3.3) in terms of the overall chain stretch

[10] We use the phrases "damage variable" and "phase-field" interchangeably to describe d.
[11] We do not consider "healing," that is $\dot{\mathrm{d}} < 0$, in this paper.

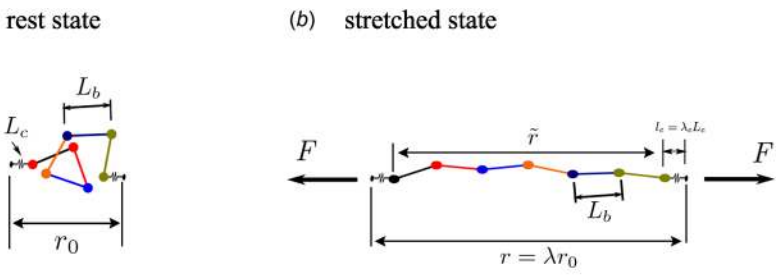

Fig. 1 Schematic of a single chain with weak crosslinks at each end: (*a*) rest state and (*b*) stretched state. The Kuhn segments are assumed to be rigid while the crosslinks are assumed to be deformable.

$$\lambda = \frac{r}{r_0} \tag{3.5}$$

where r_0, the unstretched chain length, which is now given by

$$r_0 = \sqrt{n}L_b + 2L_c \tag{3.6}$$

Thus, using Eqs. (3.4)–(3.6), we have

$$\frac{\tilde{r}}{nL_b} = \frac{\lambda}{\sqrt{n}} - \frac{2L_c}{nL_b}(\lambda_c - \lambda) \tag{3.7}$$

On physical grounds, we require that

$$\frac{\tilde{r}}{nL_b} \to \frac{\lambda}{\sqrt{n}} \quad \text{as} \quad \lambda_c \to 1, \tag{3.8}$$

so that the free energy expression (3.3) reduces to the classical expression (3.1). However, as it stands use of the estimate Eq. (3.7) in Eq. (3.3) does not give the desired limit. To achieve this, we subtract a small term

$$\frac{2L_c}{nL_b}(\lambda - 1) \tag{3.9}$$

from the right-hand side of Eq. (3.7) to obtain a slightly modified estimate

$$\frac{\tilde{r}}{nL_b} = \frac{\lambda}{\sqrt{n}} - \frac{2L_c}{nL_b}(\lambda_c - 1) \tag{3.10}$$

We consider the term (3.9) to be "small" because the coefficient $(2L_c)/(nL_b)$ is small. Typically, the statistical segment length L_b is approximately 5 to 10 times the length of a backbone bond within the polymer chain ($\approx$0.15 nm), and the effective length L_c of a crosslink is of the same order as the length of a backbone bond; this gives $(L_c/L_b) \sim 0.1$ to 0.2. Also, n is much larger than unity, and $(\lambda - 1)/n$ is small.

Finally, using Eq. (3.10) in (3.3) leads to

$$\begin{aligned}\psi &= \hat{\psi}(\lambda, \lambda_c) \\ &= \underbrace{2\hat{\varepsilon}_c(\lambda_c)}_{\hat{\varepsilon}^0(\lambda_c)} + \underbrace{k_B\vartheta n\left[\left(\frac{\lambda}{\sqrt{n}} - \frac{2L_c(\lambda_c - 1)}{nL_b}\right)\beta + \ln\left(\frac{\beta}{\sinh\beta}\right)\right]}_{-\vartheta\hat{\eta}(\lambda,\lambda_c)}, \text{ with} \\ \beta &= \mathcal{L}^{-1}\left(\frac{\lambda}{\sqrt{n}} - \frac{2L_c(\lambda_c - 1)}{nL_b}\right)\end{aligned} \tag{3.11}$$

Here, the first term denotes the internal energy associated with the stretching of the crosslinks, and the second term is for the configurational entropy associated with Kuhn segments.

At any *fixed* stretch λ, increasing λ_c increases the internal energy contribution to the free energy while decreasing the entropic part. This competition induces an optimal value of λ_c which will minimize the free energy and will be the actual state adopted by the system. Thus, setting $\partial\psi/\partial\lambda_c = 0$ provides an implicit equation for λ_c, which reads

$$\frac{\mathrm{d}\hat{\varepsilon}_c(\lambda_c)}{\mathrm{d}\lambda_c} - k_B\vartheta\frac{L_c}{L_b}\mathcal{L}^{-1}\left(\frac{\lambda}{\sqrt{n}} - \frac{2L_c(\lambda_c - 1)}{nL_b}\right) = 0 \tag{3.12}$$

Remark 1. It is possible to build a crosslinked polymer chain network with a unit comprising a chain of n rigid Kuhn segments, each of fixed length L_b, with a *single* crosslinker of length L_c, instead of two crosslinkers as considered above. A conceptually simple way to reconcile the one crosslink model with the two crosslink model is to consider the single crosslink to be divided into two, and distributed at each end of a chain. Mathematically, the only difference in the model based on one versus two crosslinks per chain is the factor of 2 appearing in the terms

$$2\hat{\varepsilon}_c(\lambda_c) \quad \text{and} \quad \frac{2L_c}{L_b}\frac{(\lambda_c - 1)}{n}$$

in Eq. (3.11). The factor of 2 in $2\hat{\varepsilon}_c(\lambda_c)$ is inconsequential; it can easily be absorbed in the unspecified function $\hat{\varepsilon}_c(\lambda_c)$, and we may redefine $2L_c$ as L_c, to arrive at a free energy expression corresponding to a one crosslink per chain model.

3.2 Deformation, Damage, and Failure of a Crosslinked Network of Polymer Chains. We employ the widely used Arruda–Boyce [17] model to extend the single chain model to a continuum model for a polymer network. To this end, we follow Anand [18] and define the effective chain stretch

$$\bar{\lambda} \overset{\text{def}}{=} \sqrt{\mathrm{tr}\bar{\mathbf{C}}/3} \tag{3.13}$$

where $\mathrm{tr}(\cdot)$ represents the trace of a second-order tensor, $\bar{\mathbf{C}} = \bar{\mathbf{F}}^{\top}\bar{\mathbf{F}}$ is the distortional right Cauchy–Green tensor, and $\bar{\mathbf{F}} = (\det\mathbf{F})^{-1/3}\mathbf{F}$ is the distortional part of the deformation gradient. Then, with

- N representing the number of chains per unit volume of the reference configuration,

the entropy density of the network is given by

$$\begin{aligned}\eta_R &= \hat{\eta}_R(\bar{\lambda}, \lambda_c) = -Nk_B n\left[\left(\frac{\bar{\lambda}}{\sqrt{n}} - \frac{2L_c(\lambda_c - 1)}{nL_b}\right)\beta + \ln\left(\frac{\beta}{\sinh\beta}\right)\right], \\ \beta &= \mathcal{L}^{-1}\left(\frac{\bar{\lambda}}{\sqrt{n}} - \frac{2L_c(\lambda_c - 1)}{nL_b}\right)\end{aligned} \tag{3.14}$$

where

- L_b is the *statistical segment length* of a rigid-link of the chain, and

- L_c is an effective length of a crosslink.

As mentioned previously, typically the statistical segment length L_b is about 5 to 10 times the length of a backbone bond within the polymer chain ($\approx$0.15 nm), and the effective length L_c of a crosslink is of the same order as the length of a backbone bond.

Also, the internal energy density ε_{R} of the network is taken to depend on λ_c, a damage variable d and its gradient ∇d, and we also allow for internal energy contribution due to volume ratio J

$$\varepsilon_{\mathrm{R}} = \hat{\varepsilon}_{\mathrm{R}}(\lambda_c, J, \mathrm{d}, \nabla \mathrm{d}) = g(\mathrm{d})\hat{\varepsilon}^0_{\mathrm{R}}(\lambda_c, J) + \hat{\varepsilon}_{\mathrm{R,nonloc}}(\nabla \mathrm{d}) \tag{3.15}$$

We consider the following specializations for the different terms in the expression (3.15) for the internal energy per unit reference volume:

(i) The term $\hat{\varepsilon}^0_{\mathrm{R}}(\lambda_c, J)$ represents an *undamaged* internal energy per unit reference volume for which we choose a simple constitutive relation of the form

$$\hat{\varepsilon}^0_{\mathrm{R}}(\lambda_c, J) = \frac{1}{2} N_c E_c (\lambda_c - 1)^2 + \underbrace{\frac{1}{2} K (J-1)^2}_{\hat{\varepsilon}_{\mathrm{Rv}}(J)} \tag{3.16}$$

where,

- E_c represents a stiffness of the crosslinks;
- N_c is the number of crosslinks per unit reference volume, with $N_c \lessapprox N$; and
- K a bulk modulus for the network to account for intermolecular interactions and a slight compressibility of the material.[12]

(ii) The function $g(\mathrm{d})$ is a monotonically decreasing *degradation function* with values

$$g(0) = 1, \quad g(1) = 0, \quad \text{and} \quad g'(1) = 0$$

A widely used degradation function is

$$g(\mathrm{d}) = (1 - \mathrm{d})^2 \tag{3.17}$$

we adopt it here.

(iii) The term $\hat{\varepsilon}_{\mathrm{R,nonloc}}(\nabla \mathrm{d})$ in the internal energy density is a nonlocal contribution

$$\hat{\varepsilon}_{\mathrm{R,nonloc}}(\nabla \mathrm{d}) = \frac{1}{2} \varepsilon^f_{\mathrm{R}} \ell^2 |\nabla \mathrm{d}|^2 \tag{3.18}$$

where ℓ represents an intrinsic length scale for the damage process, and

$$\varepsilon^f_{\mathrm{R}} \stackrel{\mathrm{def}}{=} N_c \varepsilon^f_c \tag{3.19}$$

represents the energy of crosslink scission per unit volume when all crosslinks are broken.[13]

With the constitutive relations (3.14)–(3.19) for ε_{R} and η_{R} in hand, the free energy $\psi_{\mathrm{R}} = \varepsilon_{\mathrm{R}} - \vartheta \eta_{\mathrm{R}}$ is given by

$$\begin{aligned}\psi_{\mathrm{R}} &= (1-\mathrm{d})^2 \left(\frac{1}{2} \bar{E}_c (\lambda_c - 1)^2 + \frac{1}{2} K (J-1)^2 \right) \\ &\quad + \mathrm{G}_0\, n \left[\left(\frac{\bar{\lambda}}{\sqrt{n}} - \frac{2L_c(\lambda_c - 1)}{nL_b} \right) \beta + \ln \left(\frac{\beta}{\sinh \beta} \right) \right], \\ &\quad + \frac{1}{2} \varepsilon^f_{\mathrm{R}} \ell^2 |\nabla \mathrm{d}|^2, \quad \text{with} \quad \beta = \mathcal{L}^{-1} \left(\frac{\bar{\lambda}}{\sqrt{n}} - \frac{2L_c(\lambda_c - 1)}{nL_b} \right)\end{aligned} \tag{3.20}$$

where we have introduced the notations

$$G_0 \stackrel{\mathrm{def}}{=} N k_{\mathrm{B}} \vartheta \quad \text{and} \quad \bar{E}_c \stackrel{\mathrm{def}}{=} N_c E_c \tag{3.21}$$

with G_0 representing the ground-state shear modulus for the polymer network, and $\bar{E}_c$ a crosslink stiffness parameter for the network.

Using this free energy, Eq. (3.20) and equations (2.2) give the Piola stress $\mathbf{T}_{\mathrm{R}}$ as

$$\mathbf{T}_{\mathrm{R}} = \bar{G} \left(J^{-2/3} \mathbf{F} - \bar{\lambda}^2 \mathbf{F}^{-\top} \right) + (1-\mathrm{d})^2 K (J-1) J \mathbf{F}^{-\top}, \quad \text{where}$$

$$\bar{G} = \mathrm{def}\, G_0 \left(\frac{\sqrt{n}}{3\bar{\lambda}} \right) \mathcal{L}^{-1} \left(\frac{\bar{\lambda}}{\sqrt{n}} - \frac{2L_c(\lambda_c - 1)}{nL_b} \right) \tag{3.22}$$

is a generalized shear modulus. Also, Eq. (2.3) gives that the effective crosslink stretch λ_c is determined by solving the implicit equation

$$(1-\mathrm{d})^2 \bar{E}_c (\lambda_c - 1) - 2G_0 \frac{L_c}{L_b} \mathcal{L}^{-1} \left(\frac{\bar{\lambda}}{\sqrt{n}} - \frac{2L_c(\lambda_c - 1)}{nL_b} \right) = 0 \tag{3.23}$$

Note that generalized shear modulus $\bar{G}$ is connected to the damage field d implicitly through Eq. (3.23) for λ_c.

To complete the specification of the constitutive relations, we specify the dissipative microforce ϖ_{diss} that expends power through $\dot{\mathrm{d}}$.[14] The dissipative microforce is partitioned into a rate-independent part and a rate-dependent part through

$$\varpi_{\mathrm{diss}} = \underbrace{\alpha}_{\mathrm{rate-independent}} + \underbrace{\zeta \dot{\mathrm{d}}}_{\mathrm{rate-dependent}} \tag{3.24}$$

The rate-independent part of the dissipative microforce α is the sum of the contributions from each crosslink and given by Eq. (3.19), thus

$$\alpha = \varepsilon^f_{\mathrm{R}} \tag{3.25}$$

The rate-dependent contribution to the dissipative microforce $\zeta \dot{d}$ is simply described by a constant kinetic modulus $\zeta > 0$, with the rate-independent limit of damage evolution given by $\zeta \to 0$.

Using the specializations above, the microforce balance (2.8), which gives the evolution of d, becomes

$$\zeta \dot{\mathrm{d}} = 2(1-\mathrm{d}) \hat{\varepsilon}^0_{\mathrm{R}}(\lambda_c, J) + \varepsilon^f_{\mathrm{R}} \ell^2 \Delta \mathrm{d} - \varepsilon^f_{\mathrm{R}} \tag{3.26}$$

The microforce balance (3.26) can be rewritten to enforce the constraint $d \in [0, 1]$ in a simple way. Add and subtract the term $\varepsilon^f_{\mathrm{R}} d$ to get

[12]The particular form of the volumetric internal energy is not crucial for elastomers in which the volume changes due to intermolecular interactions are typically quite small relative to distortional deformations. In our finite element simulations, we encountered some convergence difficulties with the simple quadratic form $\hat{\varepsilon}_{\mathrm{Rv}}(J) = 1/2K(J-1)^2$ of the volumetric internal energy at late stages of the damage. Accordingly, in our computations, we have used the alternate form $\hat{\varepsilon}_{\mathrm{Rv}}(J) = K/8(J - J^{-1})^2$, which reduces to a simple quadratic energy as $J \to 1$ $\hat{\varepsilon}_{\mathrm{Rv}}(J) = \frac{K}{8}(J - J^{-1})^2 = \frac{K}{8}(J-1)^2\left(1 + \frac{1}{J}\right)^2 \approx \frac{1}{2}K(J-1)^2$ If for some numerical reason J becomes large during the iteration process, then the alternate form leads to a softer response [19].

[13]In formulating a theory that accounts for the stretching and failure of the crosslinks, we have assumed that all crosslinks in a continuum material point are uniformly stretched and that they fail simultaneously. This is clearly a major approximation since the actual failure process is expected to be stochastic in nature, with the weakest link failing first.

[14]Cf. Eq. (2.5).

$$\zeta\dot{\mathrm{d}} = 2(1-\mathrm{d})(\hat{\varepsilon}^0_{\mathrm{R}}(\lambda_c, J) - \varepsilon^f_{\mathrm{R}}/2) - \varepsilon^f_{\mathrm{R}} d + \varepsilon^f_{\mathrm{R}}\ell^2\Delta\mathrm{d} \tag{3.27}$$

The constraint $d \in [0,1]$ is automatically satisfied if the equation above is modified to read as

$$\zeta\dot{\mathrm{d}} = 2(1-\mathrm{d})\langle\hat{\varepsilon}^0_{\mathrm{R}}(\lambda_c, J) - \varepsilon^f_{\mathrm{R}}/2\rangle - \varepsilon^f_{\mathrm{R}}(\mathrm{d} - \ell^2\Delta\mathrm{d}) \tag{3.28}$$

where $\langle\bullet\rangle$ are Macaulay brackets, i.e.,

$$\langle x\rangle = \begin{cases} 0, & x < 0 \\ x, & x \geq 0 \end{cases}$$

At this stage, the irreversible nature of crosslink scission is not yet reflected in the model. To this end, we replace the term $\langle\hat{\varepsilon}^0_{\mathrm{R}}(\lambda_c, J) - \varepsilon^f_{\mathrm{R}}/2\rangle$ in the microforce balance with the monotonically increasing history field function [20]

$$\mathcal{H}(t) \stackrel{\mathrm{def}}{=} \max_{s\in[0,t]}\left\langle\hat{\varepsilon}^0_{\mathrm{R}}(\lambda_c(s), J(s)) - \varepsilon^f_{\mathrm{R}}/2\right\rangle \tag{3.29}$$

where at each $s \in [0,t]$

$$\hat{\varepsilon}^0_{\mathrm{R}}(\lambda_c(s), J(s)) = \frac{1}{2}\bar{E}_c(\lambda_c(s)-1)^2 + \frac{1}{2}K(J(s)-1)^2 \tag{3.30}$$

and

$$\varepsilon^f_{\mathrm{R}} = N_c\,\varepsilon^f_c \tag{3.31}$$

is a fracture energy. With these modifications, the evolution equation (2.8) for the damage variable d becomes

$$\zeta\dot{\mathrm{d}} = 2(1-\mathrm{d})\mathcal{H} - \varepsilon^f_{\mathrm{R}}(\mathrm{d} - \ell^2\Delta\mathrm{d}) \tag{3.32}$$

which is of a form similar to that in the paper by Miehe and Schänzel [7] on phase field modeling of fracture of rubbery polymers.

Material parameters in the theory: The theory involves the following material parameters:

$$L_b, \quad n, \quad N, \quad L_c, \quad N_c, \quad E_c, \quad K, \quad \varepsilon^f_c, \quad \ell, \quad \text{and} \quad \zeta \tag{3.33}$$

Here, L_b is the statistical length of a rigid segment in a chain, n is the number of rigid segments in a chain, N is the number of chains per unit volume, L_c is the length of a crosslink, N_c is the number of crosslinks per unit volume, E_c represents the stiffness of the crosslinks, K represents the bulk modulus of the material, ε^f_c, a crosslink dissociation energy per unit volume, ℓ is a characteristic length scale of the gradient theory under consideration; and ζ is a kinetic modulus for the evolution of the damage. All parameters are required to be positive.

In the numerical simulations described in Sec. 4, instead of the parameter list (3.33), we use the parameter list

$$L_c = 0.2L_b,\ G_0 = Nk_{\mathrm{B}}\vartheta,\ n,\ \bar{E}_c = N_cE_c,\ K,\ \varepsilon^f_{\mathrm{R}} = N_c\varepsilon^f_c,\ \ell,\ \text{and}\ \ \zeta \tag{3.34}$$

where G_0 is the ground-state shear modulus for the polymer network, $\bar{E}_c$ is a crosslink-stiffness parameter for the network, and $\varepsilon^f_{\mathrm{R}}$ represents the energy per unit volume for the dissociation of the crosslinks in a network.

3.3 Some Remarks

Remark 2. It is of interest to make a comparison between fracture resulting from the chain scission mode and that resulting from crosslink failure mode, and to identify the critical material parameters for these two competing mechanisms. To do this, we suppress the damage field d and any discussion of the final damage process. From the discussion presented in our recent papers on fracture due to the chain scission mechanism [4,5], and the discussion in Sec. 3.1 of the present paper on fracture due to crosslink failure, the free energy for a single chain *accounting for both bond stretch and crosslink stretch* may be expressed as

$$\psi = n\hat{\varepsilon}_b(\lambda_b) + 2\hat{\varepsilon}_c(\lambda_c) + nk_{\mathrm{B}}\vartheta\left[\left(\frac{\lambda}{\sqrt{n}\lambda_b} - \frac{2L_c}{nL_b}\frac{\lambda_c-1}{\lambda_b}\right)\beta + \ln\left(\frac{\beta}{\sinh\beta}\right)\right] \tag{3.35}$$

with

$$\beta = \mathcal{L}^{-1}\left(\frac{\lambda}{\sqrt{n}\lambda_b} - \frac{2L_c}{nL_b}\frac{\lambda_c-1}{\lambda_b}\right) \tag{3.36}$$

and

$$\hat{\varepsilon}_b(\lambda_b) = \frac{1}{2}E_b(\lambda_b-1)^2, \quad \hat{\varepsilon}_c(\lambda_c) = \frac{1}{2}E_c(\lambda_c-1)^2 \tag{3.37}$$

The equations that determine the bond stretch λ_b and the crosslink stretch λ_c are again obtained by minimizing the free energy with respect to these two variables

$$\frac{\partial\psi}{\partial\lambda_b} = 0, \quad \text{and} \quad \frac{\partial\psi}{\partial\lambda_c} = 0 \tag{3.38}$$

which using the free energy expression (3.35) give the following two equations to determine λ_b and λ_c

$$\begin{aligned} E_b(\lambda_b-1) &= k_{\mathrm{B}}\vartheta\beta\lambda_b^{-1}\left(\frac{\lambda}{\sqrt{n}\lambda_b} - \frac{2L_c}{nL_b}\frac{\lambda_c-1}{\lambda_b}\right), \quad \text{and} \\ E_c(\lambda_c-1) &= k_{\mathrm{B}}\vartheta\beta\left(\frac{L_c}{L_b}\right)\lambda_b^{-1} \end{aligned} \tag{3.39}$$

Next, let us consider fracture of a single chain for which the Kuhn segments and the crosslinks are allowed to stretch. Physically, as the chain is stretched, the internal energy due to bond stretch $\hat{\varepsilon}_b(\lambda_b)$ and that due to crosslink stretch $\hat{\varepsilon}_c(\lambda_c)$ will increase. The chain will fail by the chain scission mode or the crosslink failure mode depending on whether $\hat{\varepsilon}_b(\lambda_b)$ or $\hat{\varepsilon}_c(\lambda_c)$ first reach their respective dissociation energies ε^f_b and ε^f_c. To represent this competition, we introduce a positive-valued dimensionless factor

$$\gamma \stackrel{\mathrm{def}}{=} \frac{\hat{\varepsilon}_c(\lambda_c)/\varepsilon^f_c}{\hat{\varepsilon}_b(\lambda_b)/\varepsilon^f_b} \tag{3.40}$$

Thus, if $\gamma > 1$, then the energy stored in crosslink bonds will reach its critical value first, and the chain will fail by the crosslink failure mode. On the other hand, if $\gamma < 1$, then the energy stored in Kuhn segments will reach its critical value first, and the chain will fail by the chain scission mode.

By using Eq. (3.37), we may rewrite γ defined in Eq. (3.40) as

$$\gamma = \frac{E_c(\lambda_c-1)^2}{E_b(\lambda_b-1)^2}\left(\frac{\varepsilon^f_b}{\varepsilon^f_c}\right) = \frac{E_c^2(\lambda_c-1)^2}{E_b^2(\lambda_b-1)^2}\left(\frac{E_b}{E_c}\right)\left(\frac{\varepsilon^f_b}{\varepsilon^f_c}\right) \tag{3.41}$$

Next, using Eq. (3.39), we write γ alternatively as

$$\gamma = \left(\frac{\lambda}{\sqrt{n}\lambda_b} - \frac{2L_c}{nL_b}\frac{\lambda_c-1}{\lambda_b}\right)^{-2}\left(\frac{L_c}{L_b}\right)^2\left(\frac{E_b}{E_c}\right)\left(\frac{\varepsilon^f_b}{\varepsilon^f_c}\right) \tag{3.42}$$

Physically, when failure occurs, by either failure mode, the quantity $((\lambda/\sqrt{n}\lambda_b) - (2L_c/nL_b)(\lambda_c - 1/\lambda_b))$ in Eq. (3.42) is very close to unity, and hence

$$\gamma \approx \left(\frac{L_c}{L_b}\right)^2\left(\frac{E_b}{E_c}\right)\left(\frac{\varepsilon^f_b}{\varepsilon^f_c}\right) \tag{3.43}$$

Thus, by using straightforward scaling relations in going from a single chain to a polymer network (as we did in Sec. 3.2), we may rewrite γ as

$$\gamma \approx \left(\frac{N_c L_c}{nNL_b}\right)^2 \left(\frac{\bar{E}_b}{\bar{E}_c}\right) \left(\frac{\varepsilon^f_{\mathrm{R},b}}{\varepsilon^f_{\mathrm{R},c}}\right) \tag{3.44}$$

This expression for γ reveals the material parameters in a polymer network, which control the competition between the crosslink failure mechanism and the chain scission failure mechanism. If one knows the values of the material parameters in Eq. (3.44) for a specific material, then one can determine the failure mode of the material:

- If $\gamma > 1$, then the network will fail by the crosslink failure mode.
- If $\gamma < 1$, then the network will fail by the chain scission failure mode.

Remark 3. A macroscopic critical energy release rate G_c may be estimated if the crosslinks are sufficiently strong. In this case, the internal energy will significantly outweigh the entropic part of the free energy at the point of crosslink failure, and thus the entropic free energy contribution to the energy release rate will be negligible. In our gradient-damage model, the dissipation scales as $\varepsilon^f_{\mathrm{R}}\ell^3$, while for a theoretical sharp crack it would scale as $G_c\ell^2$ so that

$$\varepsilon^f_{\mathrm{R}} \times \ell \approx G_c \tag{3.45}$$

Remark 4. The overall response of our new model for fracture of polymers due to crosslink failure is similar to that in our recent papers, which focused on a model for failure of polymers due to chain scission [4,5]. However, because of the intrinsic physical differences embedded in these two models, there is an important difference in the consequences from these two models regarding the scaling of G_c with microstructural parameters. Specifically:

- The internal energy in our previous model for fracture by chain scission reads as

$$\varepsilon^f_{\mathrm{R}} = Nn\varepsilon^f_b \tag{3.46}$$

where ε^f_b is a bond dissociation energy. With ρ the mass density of the polymer and m the molecular mass of a Kuhn segment, the number of chains per unit reference volume is given by $N = \rho/(mn)$ so that

$$Nn = \frac{\rho}{m} \tag{3.47}$$

Using Eq. (3.47), and an estimate for ℓ in terms of the rest length $r_0 = \sqrt{n}L_b$ of a chain

$$\ell \propto \sqrt{n}L_b \tag{3.48}$$

Equation (3.45) gives

$$G_c \propto \left(\frac{\varepsilon^f_b L_b \rho}{m}\right)\sqrt{n} \tag{3.49}$$

In this scenario, the Lake–Thomas scaling holds—the toughness G_c is proportional to $\sqrt{n}$.

As noted earlier, in their fracture experiments on Tetra-PEG gels, with precisely controlled network structures, [2] showed that

$$G_c \propto \sqrt{n}$$

which confirmed the Lake–Thomas scaling for these materials; cf. Fig. 8 of Ref. [3].[15]

Further, from Eq. (3.47) and the expression $G_0 = Nk_{\mathrm{B}}\vartheta$ for the ground-state shear modulus, we have that

$$\sqrt{n} = \sqrt{\frac{\rho}{m}}\frac{1}{\sqrt{N}} = \sqrt{\frac{\rho\, k_{\mathrm{B}}\vartheta}{m}}\frac{1}{\sqrt{G_0}} \tag{3.50}$$

use of which in Eq. (3.49) gives that

$$G_c \propto \frac{1}{\sqrt{G_0}} \tag{3.51}$$

Thus, for fixed crosslink elastomers, which fail by chain scission, there is a trade-off between toughness (fracture energy G_c) and stiffness (shear modulus G_0): by increasing the cross-linking density the initial stiffness $G_0 = Nk_{\mathrm{B}}\vartheta$ increases proportionally to the increase in the number N of chains (elastically effective strands) per unit volume, while the toughness G_c decreases owing to the decrease in the number n of monomers in a chain. As reviewed recently by Creton [12], such a trade-off between the stiffening and toughening in conventional fixed-crosslink elastomers and gels has been observed experimentally.

- However, the internal energy in the present model for fracture due to crosslink stretch and failure is

$$\varepsilon^f_{\mathrm{R}} = N_c\varepsilon^f_c \tag{3.52}$$

where ε^f_c is a crosslink dissociation energy. In this case from Eq. (3.45), with an estimate (3.48) for ℓ in terms of the rest length $r_0 = \sqrt{n}L_b$ of a chain, and with the number of crosslinks per unit reference volume N_c proportional to the number of chains per unit reference volume N

$$N_c \propto N = \frac{\rho}{mn} \tag{3.53}$$

we obtain

$$G_c \propto \left(\frac{\varepsilon^f_c L_b\, \rho}{m}\right)\frac{1}{\sqrt{n}} \tag{3.54}$$

In the crosslink failure-based micromechanism of fracture the Lake–Thomas scaling *does not hold*—the toughness G_c is proportional to $1/\sqrt{n}$ and not $\sqrt{n}$.

Further, using Eqs. (3.50), (3.54) implies that

$$G_c \propto \sqrt{G_0} \tag{3.55}$$

Thus, for stretchable crosslink elastomers, the toughness (fracture energy G_c) *increases* as the stiffness (shear modulus G_0) increases—a desirable outcome, indeed. However, as far as we know, such a scaling has not been experimentally verified in the literature for any polymer, but would indeed be a means to experimentally determine whether failure of a polymer occurs by chain scission or by crosslink failure.

In any event, our study suggests that introducing stretchable crosslinks and a crosslink failure mode in polymer networks is a potential solution to the problem of the trade-off between stiffness and toughness observed in conventional fixed-crosslink elastomers and gels.

[15]Since for swollen gels $\rho = \phi_p\rho_{\mathrm{R}}$, where ρ_{R} is the mass density in an unswollen reference configuration and ϕ_p is the polymer volume fraction, they actually showed that $G_c \propto \phi_p\sqrt{n}$ That is, swollen gels with the same number of links per chain, n, have a lower toughness than the dry elastomer.

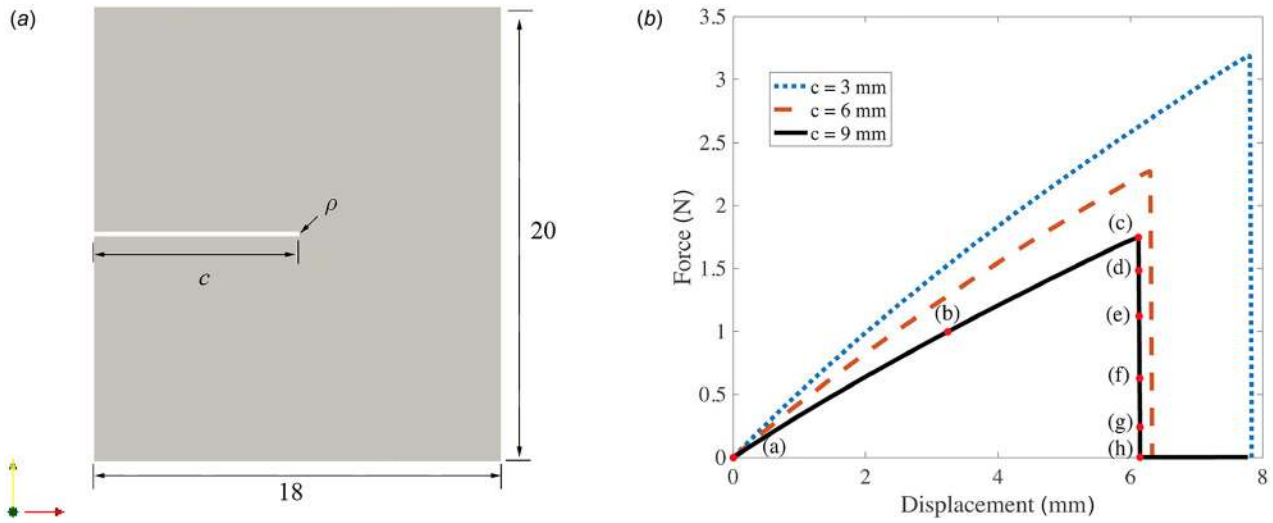

Fig. 2 (*a*) Schematic of the single-edge-notch specimen geometry; all dimensions are in mm. The thickness of the sample is 1 mm; the notch length is denoted by *c*; and $\rho = 0.1$ mm is the notch-root radius. (*b*) Calculated force–displacement curves for $c = 3, 6, 9$ mm. Contour plots for the damage variable d at points (*a*)–(*h*) on the load displacement curve for a specimen with $c = 9$ mm are shown in Fig. 3.

4 Application of the Theory to Study Plane-Stress Fracture of Elastomers

We have numerically implemented our theory in the open-source finite element code MOOSE [21] by writing our own application to solve three-dimensional, plane strain, plane-stress, axisymmetric problems. MOOSE uses a sophisticated nonlinear solver technology, and it may be massively parallelized. Using this new numerical capability, in this section, we report on some representative simulations of deformation and fracture of an elastomeric material. Specifically, we study the capability of the model to describe *plane stress* fracture of

(i) single-edge-notched specimens;
(ii) an asymmetric double-edge-notched specimen; and
(iii) fracture of a sheet specimen with multiple circular and elliptical holes.

All simulations were performed on a parallelized linux cluster. Visualization of the results was performed by using the open-source code ParaView [22].

Remark 5. In our gradient-damage theory, the free energy has a contribution (3.18) in which ε_R^f represents the energy of crosslink scission per unit volume, and ℓ is a length scale to account for gradient effects in the damage field d. Theoretically, ℓ is an intrinsic material parameter of the theory. Actual values of ℓ in elastomeric materials are expected to be $\ell \lessapprox 1\,\mu$m. For such a value of ℓ, to numerically resolve regions of sharp gradients in the damage variable d, the finite element size h_e must be much smaller than ℓ—typically $h_e \lessapprox \ell/5$—so that $h_e \lessapprox 200$ nm, which is *exceedingly small*. Use of such a small element size in the damage zone is computationally tractable (on our computers) if the in-plane dimensions of a single-edge-notched specimen are less than 1 mm, and an edge crack is a few microns is size. However, if one is interested in simulating the fracture of specimens, which have a macroscopic in-plane dimensions of say 10 mm or larger, then use of such a small value of ℓ, and therefore a small value of h_e, will result in prohibitively expensive simulations. Under these circumstances, for pragmatic reasons, ℓ may be considered a regularization parameter for the gradient-damage theory. Corresponding to a small but computationally tractable mesh size h_e selected for macroscopic-dimensioned specimens, a suitably large value of ℓ may be chosen, and the value of ε_R^f suitable reduced so that $\varepsilon_R^f \times \ell \approx G_c$, where G_c is the value of experimentally measured macroscopic critical energy release rate for a given material. *We take this pragmatic approach for the numerical simulations shown in this section.*

4.1 Single-Edge-Notch Mode-I Loading Under Plane-Stress Conditions With Different Notch Lengths. We begin with a study of fracture in single-edge-notch specimens with different crack lengths, under plane stress mode-I loading conditions. Figure 2(*a*) shows a schematic of the specimen geometry. The overall size of the notched sheet sample is 18 mm × 20 mm in the plane, and the sheet is 1 mm thick. We consider specimens with notch lengths $c = 3$, 6, and 9 mm; the initial root-radius of the notch is fixed at 0.1 mm. The material parameters used in our simulations are shown in Table 1. In our simulation, we utilize the symmetry of the geometry and the middle edge of the specimen is fixed, while the top edge is prescribed a displacement at a nominal stretch rate $\dot{\lambda} = 1 \times 10^{-3}/\text{s}$.

Some remarks concerning the choice of material parameters:

(1) We picked a round number of $G_c = 100\,\text{J/m}^2$ as a representative value of toughness for elastomeric materials. Further, in order to make the simulations numerically tractable we set the length scale to be $\ell = 100\,\mu$m. Then Eq. (3.45) gives $\varepsilon_R^f = 1.0$ MPa, as listed in Table 1.
(2) The kinetic modulus ζ, which has units of Pa·s, may be thought of as a viscous regularization parameter for an essentially rate-independent damage process, and ζ/G_0 therefore represents a time constant in the theory. For a given macroscopic stretch-rate $\dot{\lambda}$, our numerical experiments have shown that a value of ζ, which is commensurate with $(\zeta\dot{\lambda}/G_0) \lessapprox 10^{-3}$ is small enough to give an almost rate-independent damage evolution. For the values of ζ and G_0 listed in Table 1 and a nominal stretch rate $\dot{\lambda} = 1 \times 10^{-3}/\text{s}$, we have $(\zeta\dot{\lambda}/G_0) = 5 \times 10^{-5}$ which well approximates a rate-independent damage evolution response.

Table 1 Representative values of the material parameters used in the simulations

$G_0 = Nk_B\vartheta$	n	$\bar{E}_c = N_c E_c$	K	$\varepsilon_R^f = N_c\varepsilon_c^f$	ℓ	ζ
0.2 MPa	4	0.2 MPa	20 MPa	1 MPa	100 μm	10 kPa·s

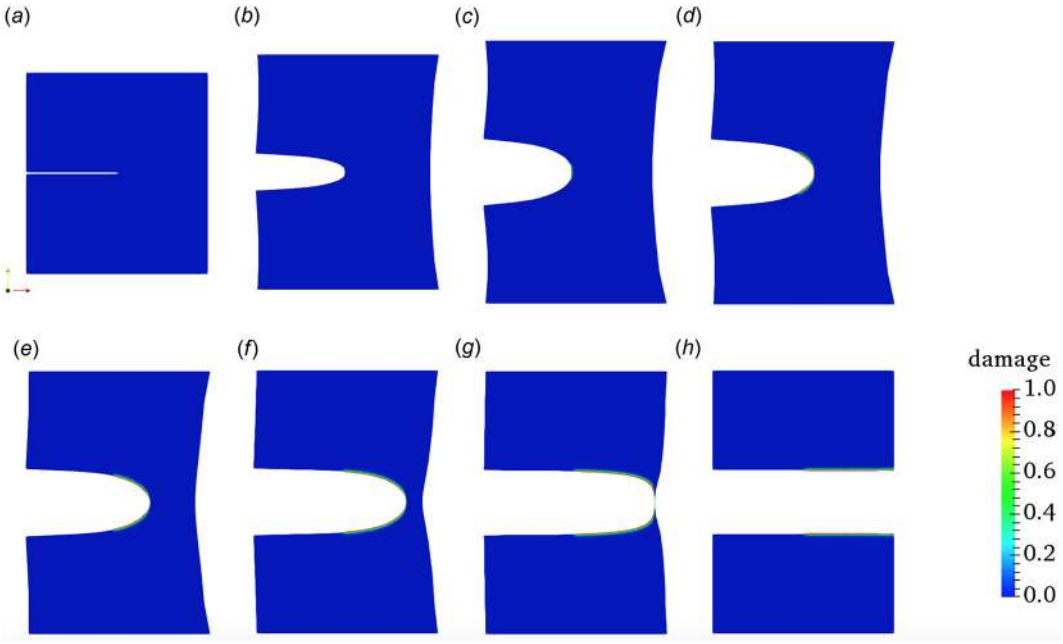

Fig. 3 Images of the deformed geometry with contour plots of the damage variable d. To aid visualization of the damage, elements with an average value of d>0.99 are removed from the plots. Since the length scale $\ell = 100\,\mu$m is very small when compared with the overall dimension of the specimen (~20 mm), the damage zone is barely visibly in this this sequence of contour plots for d.

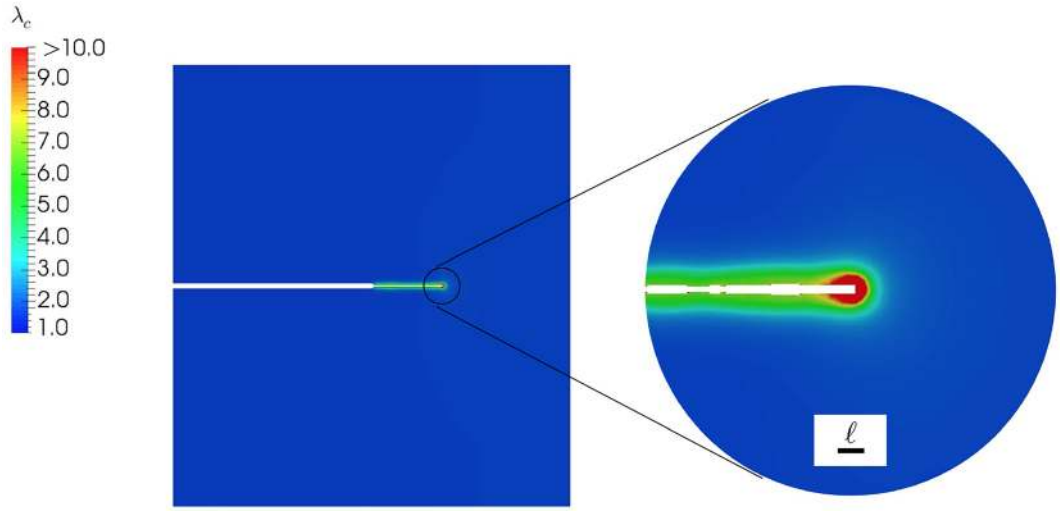

Fig. 4 Contours of crosslink stretch λ_c during the fracture process in a specimen with $c = 9$ mm. The crosslink stretch is appreciable only in a small zone near the crack tip. The contours are plotted on the reference configuration. Elements with d>0.99 are removed from the visualization.

(3) We have used a value of the bulk modulus K which is 100 times larger than the ground state shear modulus G_0; this corresponds to a ground-state Poisson's ratio of $\nu = 0.495$, which approximates an elastically incompressible material. We tried using larger values of K relative to that of G_0, but that slowed down our numerical procedures considerably. So, in all the calculations reported in this paper, we have used $K/G_0 = 100$.
(4) We have intentionally chosen a small value $n = 4$ for the number of links in the chain to illustrate the features of our theory so that failure of the chains in our simulations occurs at reasonable levels of macroscopic stretch.

Figure 2(*b*) shows the calculated force–displacement curves for cracks with initial lengths of $c = 3$, 6, 9 mm. As expected, as the initial length of the crack increases the overall force level becomes lower, and the stretch at which final fracture occurs becomes smaller. Contour plots for the damage variable d at points (*a*)–(*h*) on the load displacement curve for a specimen with $c = 9$ mm are shown in Fig. 3.

Figure 3 shows the deformed geometry at points (*a*)–(*h*) on the force–displacement curve in Fig. 2(*b*), together with contours of the damage variable d. To aid visualization of the damage, elements with an average value of $d > 0.99$ are not plotted.[16] Since the length scale $\ell = 100\ \mu$m is very small when compared with the

[16]See the Appendix, which gives an example of contour plots with and without severely damaged elements.

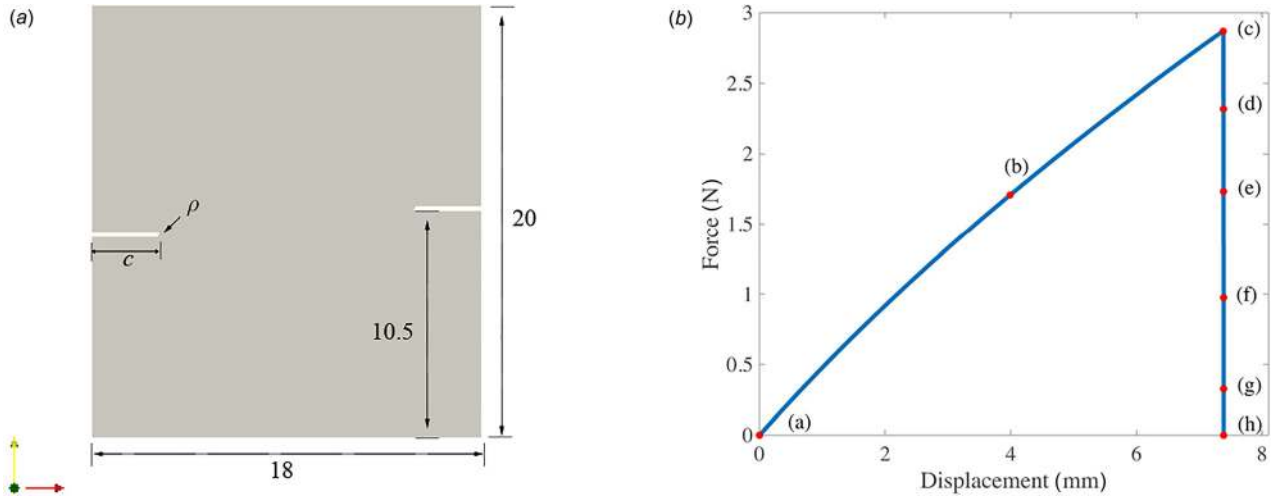

Fig. 5 (*a*) Schematic of the asymmetric-double-edge-notch specimen geometry; all dimensions are in mm. The thickness of the sample is 1 mm; the notches are of length $c = 3$ mm; and $\rho = 0.1$ mm is the notch-root radius. (*b*) Calculated force–displacement curve. The contour plots for the damage variable d at points (*a*)–(*j*) on the load displacement curve are shown in Fig. 6.

overall dimension of the specimen (∼20 mm), the damage zone is barely visibly in this sequence of plots. Figure 3(*a*) is the initial configuration. As the sample is stretched to (*b*) the notch is blunted, but no damage has initiated. Damage initiates when the sample is stretched further to a displacement level of ∼5.5 mm (a point just before (*c*)), but the force is still increasing, and it is after another ∼0.5 mm of extension that the force reaches a peak at point (*c*) in force–displacement curve, and from the contour of damage shown in Fig. 3(*c*), a small damage zone ahead of the crack becomes observable. Further stretching begins the rupture process, and Figs. 3(*d*)–3(*h*) show this progressive rupturing, with (*h*) showing the final failed configuration. Note from Fig. 2(*b*) that the force at stage (*h*) stage is essentially zero.

Figure 4 shows a contour plot of the crosslink stretch, λ_c, at a particular stage of the failure process for a specimen with an initial notch depth of $c = 9$ mm. The crack has propagated almost halfway through the remaining ligament of the specimen. The contours are plotted on the reference configuration in order to highlight the extent of crack propagation relative to the initial specimen geometry. Also, the highly damaged elements ($d > 0.99$) are again hidden from view. When failure occurs for a large sample, the deformation localizes to a small region in the vicinity of the crack-tip. In this region, the effective stretch $\bar{\lambda}$ can be very large, and λ_c will increase to the level of $\bar{\lambda}(\sqrt{n}L_b/2L_c)$, which is also very large. Therefore, in order to visualize the contours of λ_c, we have set the maximum value of the contour in λ_c to 10. As is clear from Fig. 4, the region of high

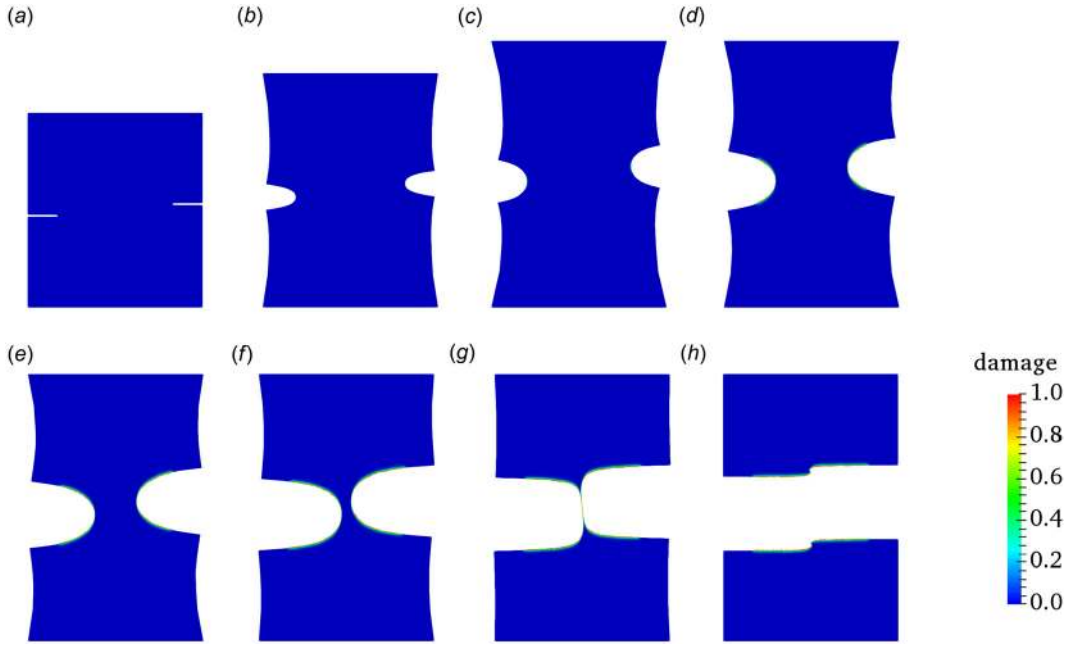

Fig. 6 The deformed geometry with contour plots of the damage variable d. To aid visualization of the damage, elements with an average value of d>0.99 are removed from the plots. Since the length scale $\ell = 100\,\mu$ m is very small compared with the overall dimension of the specimen (∼20 mm), the damage zone is barely visibly in this sequence of plots.

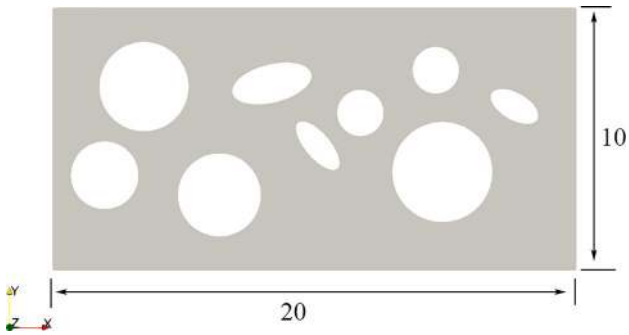

Fig. 7 Schematic of the geometry of specimen with several circular and elliptical holes; all dimensions are in mm. The thickness of the sample is 1 mm.

crosslink stretch is limited to a small region in the vicinity of the crack tip, on a scale comparable to the length scale ℓ, while the majority of the specimen displays negligible crosslink stretching.

4.2 Fracture in an Asymmetric-Double-Edge-Notched Sheet of an Elastomeric Sample Under Mode-I Plane-Stress Loading. In this section, we study fracture of an asymmetric-double-notched sheet specimen of an elastomeric sample under mode-I plane-stress loading. This example shows the powerful capability of our gradient-damage theory to model the merging of two growing cracks.

Figure 5(*a*) shows a schematic of the specimen geometry. The overall size of the double-edge-notched sheet sample is 18 mm × 20 mm in the plane, and the sheet is 1 mm thick. The two offset notches each have a of length $c = 3$ mm; the initial root-radius of the notch is 0.1 mm. We use the same values of the material parameters as in Sec. 4.1. The bottom edge of the specimen is fixed, while the top-edge is prescribed a displacement at a nominal stretch rate of 1×10^{-3}/s. Figure 5(*b*) shows the calculated force–displacement curve.

The contour plots for the damage variable, d at points (*a*)–(*h*) on the load displacement curve in Fig. 5(*b*) are shown in in Fig. 6. To aid visualization of the damage, elements with an average value of $d > 0.99$ are removed from the plots. Since the length scale $\ell = 100$ μm is very small compared with the overall dimension of the specimen (20 mm), the damage zone is barely visibly in this this sequence of plots. Figure 6(*a*) is the initial configuration. As the sample is stretched to (*b*) both the notches get blunted, but no damage has initiated. Damage initiates when the sample is stretched further to a displacement of ∼6.4 mm (just before state (*c*)), but the force is still increasing; it is only after another ∼1 mm of extension that the force reaches a peak at point (*c*) in the force–displacement curve Fig. 5(*b*), and from the contour of damage d shown in Fig. 6(*c*), a small damaged zone ahead of the crack becomes observable. Figures 6(*d*)–6(*h*) show the subsequent

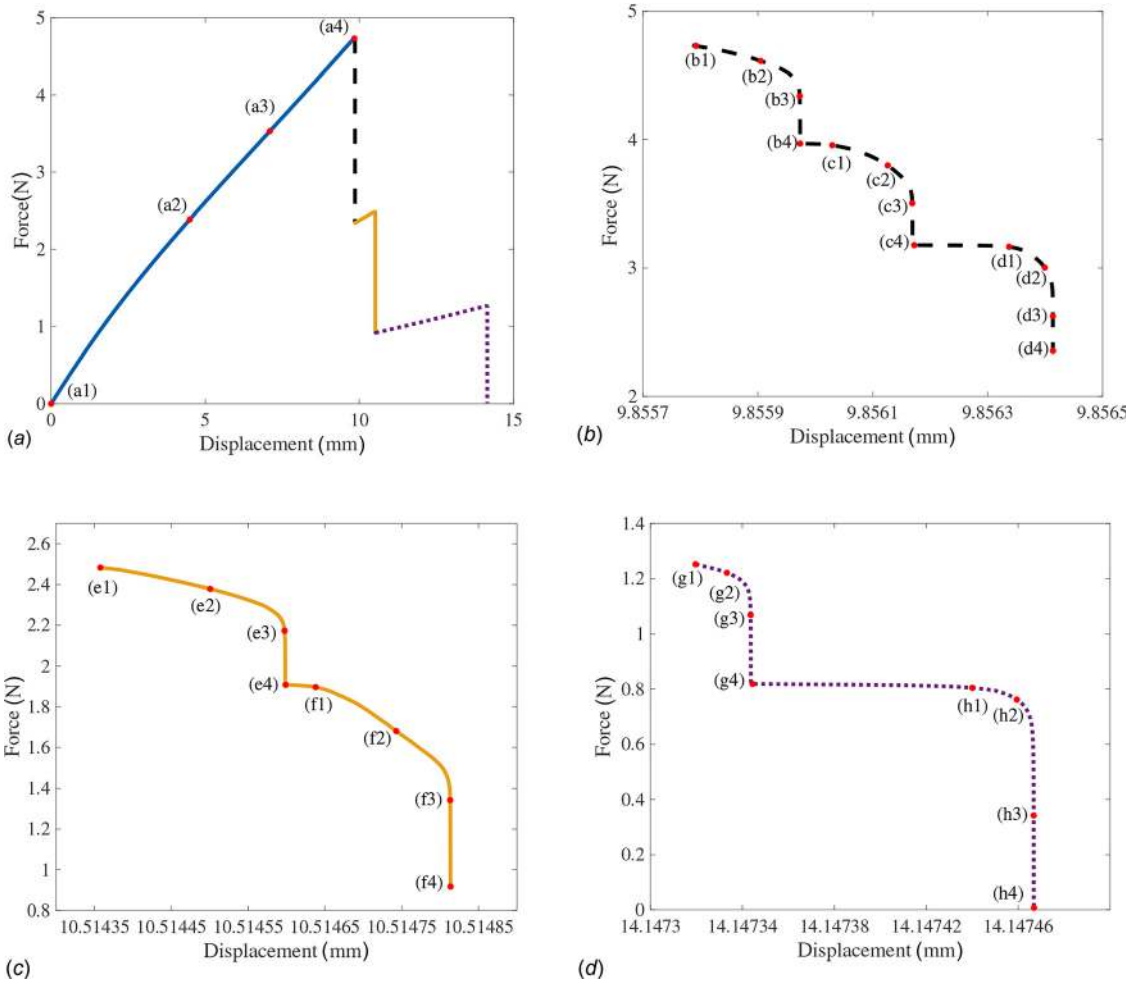

Fig. 8 (*a*) Calculated force–displacement curve. There are four different stages within the curve: (*i*) The blue line indicates the first stage. (*ii*) The dashed-black line indicates the second stage. (iii) The solid-yellow line indicates the third stage. And (iv) the dotted-pink line indicates the fourth stage. (*b*)–(*d*) show zoom-in figures for the corresponding force drop stages. The contour plots for the damage variable d at points (*a*)–(*h*) on the load displacement curve are shown in Figs. 9 and 10.

rupturing process on two cracks merging, with Fig. 6(*g*) showing a pinching off process, which leads to final fracture into two separate pieces, as shown in Fig. 6(*h*).

4.3 Fracture in a Sample With Several Circular and Elliptical Holes Under Plane-Stress Tension. In this section, we study fracture of a sample with several circular and elliptical holes under plane-stress tension. Sharp cracks are necessary for classical fracture mechanics analysis. However, sharp cracks are not necessary in our gradient-damage theory of fracture. This example shows the powerful capability of our gradient-damage theory to simulate the complicated fracture process of nucleation, propagation, branching, and merging of cracks in arbitrary geometries—propagating cracks are tracked automatically by the evolution of the smooth damage-field d on a fixed mesh.

Figure 7 shows a schematic of the specimen geometry. The overall size of the sample is 20 mm × 10 mm in the plane, and the sheet is 1 mm thick. We use the same values of the material parameters as in Sec. 4.1. The bottom edge of the specimen is fixed, while the top-edge is prescribed a displacement at a nominal stretch rate of 1×10^{-3}/s.

Figure 8(*a*) shows the calculated force–displacement curve. There are four different stages in the force–displacement curve:

(i) The line from (a1) to (a4) indicates the first stage. In this stage, as the specimen is stretched the force increases, and at the end of this stage the force reaches a peak and begins to drop.
(ii) The next dashed line segment indicates the second stage, and represents the initial phase of the force drop.
(iii) The next solid line segement indicates the third stage and represents the next phase of the force drop.
(iv) And the final dotted line-segement indicates the fourth stage, and represents the final phase of the force–displacement curve.

Figures 8(*b*)–8(*d*) show zoom-ins of the force decreasing portions in stages two, three, and four. Within each of these stages, there are instances in which the force–displacement curve resembles the shape of the number 7. For example, as shown in Fig. 8(*b*), there are three "7"-shaped instances in the second stage. Each 7-shaped instance corresponds to the failure of a ligament in the sample. Labels (b1)-(b4)–(h1)-(h4) marked on the force displacement curves in Figs. 8(*b*)–8(*d*) are used to indicate important frames for the failure of a specific ligament.

Contour plots for the damage variable d at points (*a*)–(*h*) on the load displacement curve for a specimen are shown in Figs. 9 and 10. To aid visualization of the damage, elements with an average value of $d > 0.99$ are not plotted. An arrow is used to indicate the ligament in which damage and rupture is occurring.

Figure 9(*a*1) shows the initial configuration. As the sample is stretched to (*a*2) and (*a*3) the holes are deformed, but no damage has initiated. Damage initiates when the sample is stretched further to a displacement level of ∼9 mm, a point just before (*a*4), but the force is still increasing. It is after another ∼0.85 mm of extension that the force reaches a peak at point (*a*4) in force–displacement curve. From the contours of the damage shown in Fig. 9(*a*4), a small damage zone indicated by an arrow becomes observable. The ligaments between the

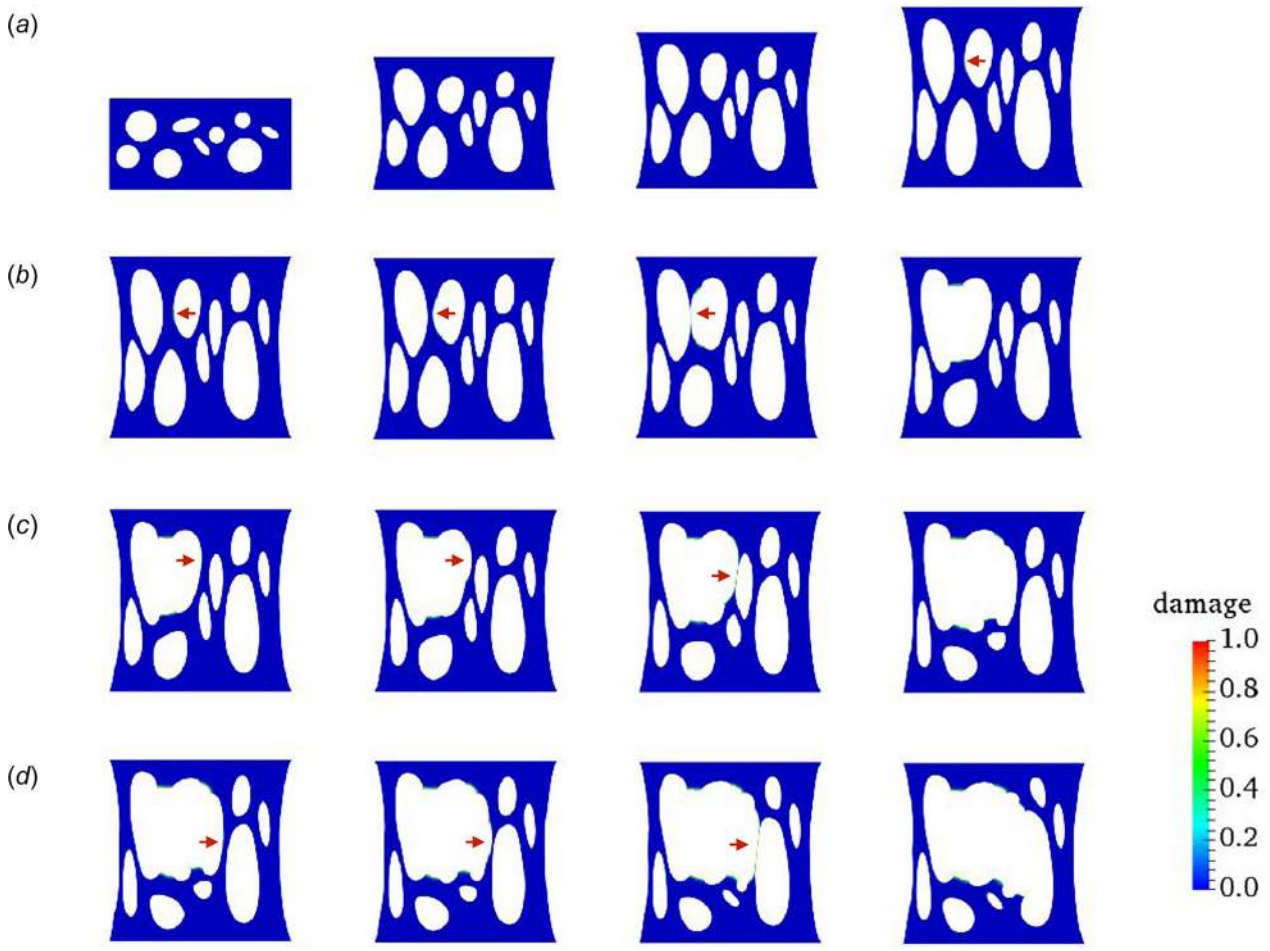

Fig. 9 Images of the deformed geometry with contour plots of the damage variable d for first and second stages. To aid visualization of the damage, elements with an average value of d>0.99 are removed from the plots. The arrows indicate the ligaments in which damage and rupture occurs.

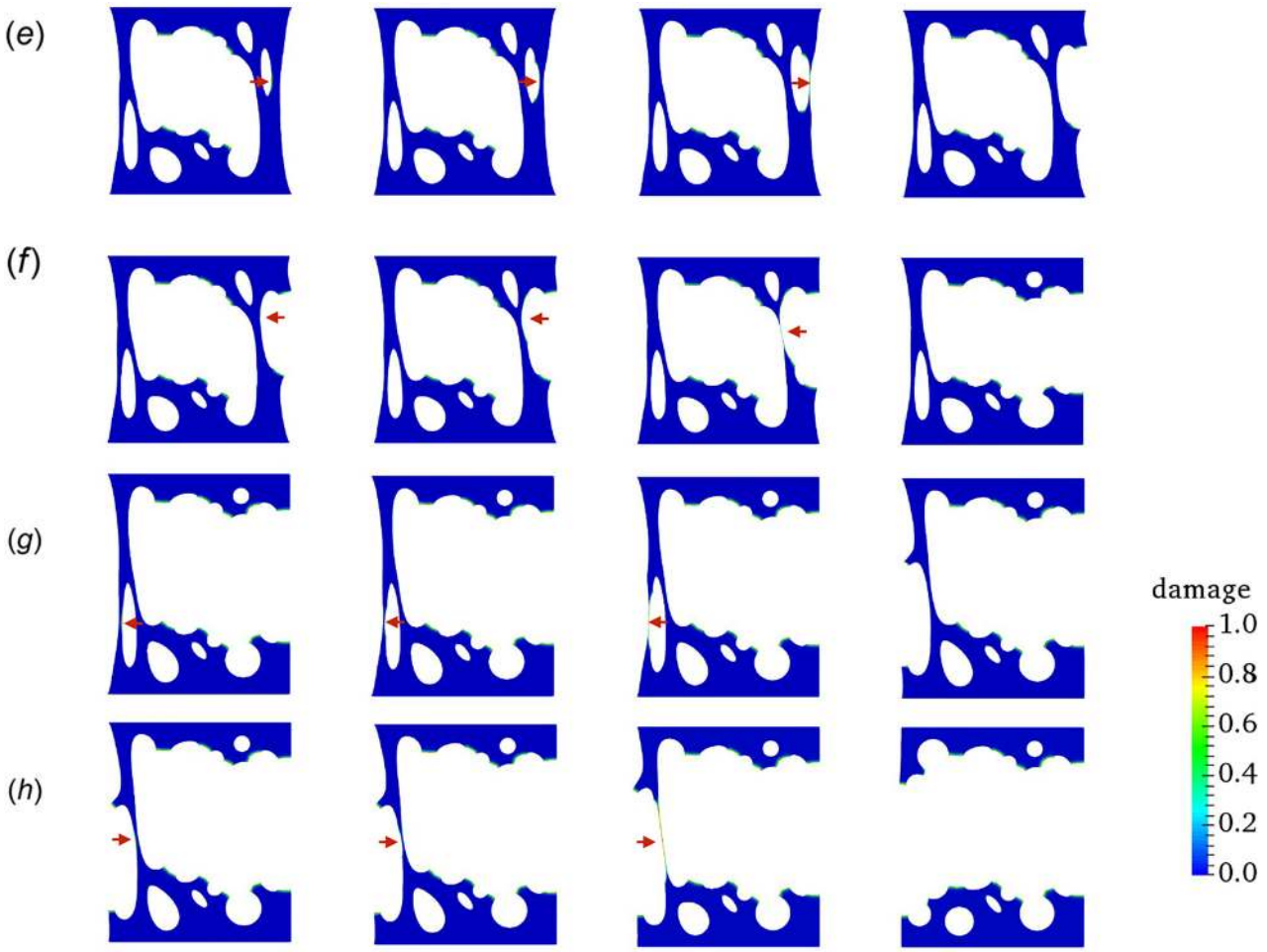

Fig. 10 Images of the deformed geometry with contour plots of the damage variable d for third and fourth stages. To aid visualization of the damage, elements with an average value of d>0.99 are removed from the plots. The arrows indicate the ligaments in which damage and rupture occurs.

holes in the soft matrix become highly stretched by point (*a*4). Further stretching begins the progressive rupture process of these ligaments.

The second stage in the force–displacement curve corresponds to failure of three ligaments, as indicated in Figs. 8(*b*) and 9(*b*)–9(*d*). In these curves, the marks (*b*1)–(*b*4), (*c*1)–(*c*4), and (*d*1)–(*d*4) are used to indicate important frames for the failure of a specific ligament. For example, in Fig. 9(*b*), the damage within a ligament indicated by the arrow is initiated in (*b*1), and (*b*2) represents a state of progressive damage of the ligament, (*b*3) shows a pinching-off process, and (*b*4) shows the total failure of the specific ligament. As the three ligaments in Figs. 9(*b*)–9(*d*) fail progressively, the cavities within the sample start to merge, and form a big cavity, cf. Fig. 9(*d*4).

After the rupture of the first three ligaments described in the paragraph above, the total displacement of the top surface is 9.85 mm; cf. Figure 8(*b*). At this point, the energy stored in the remaining ligaments is not sufficient to drive further damage. To initiate further damage, an additional macroscopic displacement

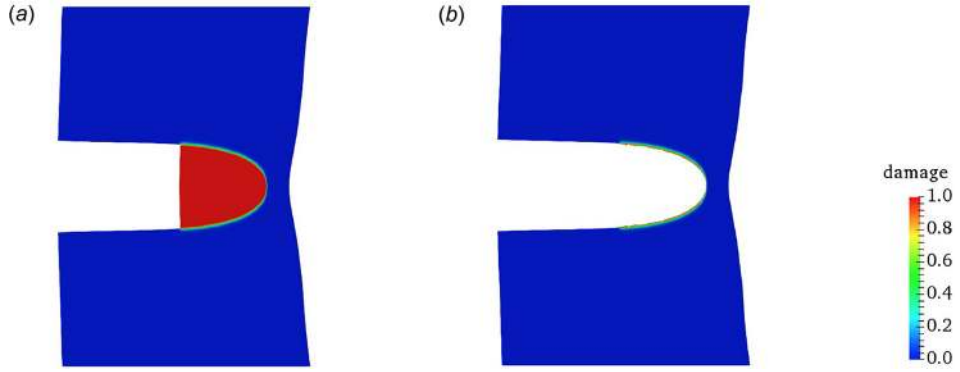

Fig. 11 (*a*) Contour plots with severely damaged elements. (*b*) The same geometry without the severely damaged elements.

of ~1 mm needs to be imposed on the sample. As this extra displacement is imposed, the remaining ligaments are further stretched and the force increases again until the beginning of the third stage; cf. Fig. 8(*a*). Upon application of this additional displacement, the stored energy within two of the remaining ligaments attains and exceeds the critical value and damage and rupture restarts, as shown in Figs. 8(*c*), 10(*e*), and 10(*f*).

After the rupture of the first five ligaments, the total displacement of the top surface is 10.514 mm; cf. Fig. 8(*c*). Again, at this point, the energy stored in the remaining two ligaments is not sufficient to drive further damage. To initiate further damage, an additional macroscopic displacement of ~3.7 mm needs to be imposed on the sample. As this extra displacement is imposed, the remaining two ligaments become highly stretched and the force again increases. The remaining ligaments accumulate energy during this additional stretching and eventually they start to damage and fail rapidly, as shown in Figs. 8(*d*), 10(*g*), and 10(*h*). Figure 10(*h*4) shows the final failed configuration.

5 Conclusions

We have formulated a theory for progressive damage and failure of elastomeric materials in which fracture occurs by crosslink failure. Specifically, we have extended the freely jointed inverse-Langevin model for a single chain, and the corresponding Arruda–Boyce [17] model for a network, to account for changes in internal energy due to stretching of the crosslinks. Crosslink damage and failure is postulated to occur upon the attainment of a critical value of the internal energy due to crosslink stretching.

We have shown in this paper that the Lake–Thomas scaling [1–3,12]—that the toughness G_c of an elastomeric material is proportional to $1/\sqrt{G_0}$, with $G_0 = Nk_B\vartheta$ the ground-state shear modulus of the material—does not hold for elastomeric materials in which fracture occurs by crosslink stretching and scission. According to our theory, for such materials, the toughness is proportional to $\sqrt{G_0}$. That is, for stretchable crosslink elastomers, the toughness increases as the stiffness increases—a desirable outcome, indeed. However, as far as we know, such a scaling has not been experimentally verified in the literature for any polymer, but would indeed be a means to experimentally determine whether failure of a polymer occurs by chain scission or by crosslink failure. In any case, our theory clearly suggests that introducing stretchable crosslinks and the crosslink failure mode in polymer networks is a potential solution to the problem of the trade-off between stiffness and toughness observed in conventional fixed-crosslink elastomers and gels.

At the continuum level, our theory is a gradient-damage or phase-field theory of fracture of elastomeric materials. We have numerically implemented this theory in an open-source finite element code MOOSE [21] by writing our own application. Using this simulation capability, we have presented results from simulations of: (i) fracture of single-edge-notched specimens; (ii) fracture of an asymmetric double-edge-notched specimen; and (iii) fracture of a sheet specimen with multiple circular and elliptical holes, under our plane stress conditions. These examples show the powerful capability of our gradient-damage theory and its numerical implementation to simulate the complicated fracture process of nucleation, propagation, branching, and merging of cracks in elastomeric materials in arbitrary geometries undergoing large deformations. We expect that our theory and numerical simulation capability will be useful in studying various interesting phenomena such as crazing and cavitation in soft materials.

In this paper, we have focused our attention on fracture of an "ideal" dry single-network elastomeric material in which fracture occurs by crosslink failure. It would be useful to extend these ideas to materials, which exhibit additional microscopic dissipation mechanisms—e.g., viscoelasticity, Mullins effect, degradation of interpenetrating networks with sacrificial bonds, fluid diffusion—that accompany the rupture process in elastomeric materials and their gels [12,14,23–25].

Acknowledgment

Support from Exxon-Mobil Research through the MIT Energy Initiative is gratefully acknowledged.

Appendix: A Contour Plots With and Without Severely Damaged Elements

In the contour plots of damage in the figures of the main text, elements with an average value of $d > 0.99$ were removed from the contour plots to aid visualization. To illustrate what we mean by this, we show in Fig. 11(*a*) a contour plot, which keeps the severely damaged elements $d > 0.99$, together with Fig. 11(*b*) the corresponding plot without the severely damaged elements.

References

[1] Lake, G. J., and Thomas, A. G., 1967, "The Strength of Highly Elastic Materials," Proc. R. Soc. London A, **300**(1460), pp. 108–119.
[2] Akagi, Y., Sakurai, H., Gong, J. P., Chung, U., and Sakai, T., 2013, "Fracture Energy of Polymer Gels With Controlled Network Structures," J. Chem. Phys., **139**(14), p. 144905.
[3] Sakai, T., 2013, "Gelation Mechanism and Mechanical Properties of Tetra-Peg Gel," Reactive Funct. Polym., **73**(7), pp. 898–903.
[4] Mao, Y., Talamini, B., and Anand, L., 2017, "Rupture of Polymers by Chain Scission," Extreme Mech. Lett., **13**, pp. 17–24.
[5] Talamini, B., Mao, Y., and Anand, L., 2018, "Progressive Damage and Rupture in Polymers," J. Mech. Phys. Solids, **111**, pp. 434–457.
[6] Grindy, S. C., Lenz, M., and Holten-Andersen, N., 2016, "Engineering Elasticity and Relaxation Time in Metal-Coordinate Cross-Linked Hydrogels," Macromolecules, **49**(21), pp. 8306–8312.
[7] Miehe, C., and Schänzel, L.-M., 2014, "Phase Field Modeling of Fracture in Rubbery Polymers—Part I: Finite Elasticity Coupled With Brittle Failure," J. Mech. Phys. Solids, **65**, pp. 93–113.
[8] Raina, A., and Miehe, C., 2016, "A Phase-Field Model for Fracture in Biological Tissues," Biomech. Model. Mechanobiol., **15**(3), pp. 479–496.
[9] Miehe, C., Welschinger, F., and Hofacker, M., 2010, "Thermodynamically Consistent Phase-Field Models of Fracture: Variational Principles and Multi-Field Fe Implementations," Int. J. Numer. Methods Eng., **83**(10), pp. 1273–1311.
[10] Bourdin, B., Francfort, G. A., and Marigo, J.-J., 2000, "Numerical Experiments in Revisited Brittle Fracture," J. Mech. Phys. Solids, **48**(4), pp. 797–826.
[11] Francfort, G. A., and Marigo, J.-J., 1998, "Revisiting Brittle Fracture as an Energy Minimization Problem," J. Mech. Phys. Solids, **46**(8), pp. 1319–1342.
[12] Creton, C., 2017, "50th Anniversary Perspective: Networks and Gels: Soft but Dynamic and Tough," Macromolecules, **50**(21), pp. 8297–8316.
[13] Gurtin, M. E., Fried, E., and Anand, L., 2010, *The Mechanics and Thermodynamics of Continua*, Cambridge University Press, New York.
[14] Mao, Y., and Anand, L., 2018, "A Theory for Fracture of Polymeric Gels," J. Phys. Mech. Solids, **115**, pp. 30–53.
[15] Kuhn, W., and Grün, F., 1942, "Beziehungen Zwischen Elastischen Konstanten Und Dehnungs-Doppelbrechung Hochelastischer Stoffe," Kolloid-Z., **101**(3), p. 248.
[16] Doi, M., 1996, *Introduction to Polymer Physics*, Oxford University Press, New York.
[17] Arruda, E. M., and Boyce, M. C., 1993, "A Three-Dimensional Constitutive Model for the Large Stretch Behavior of Rubber Elastic Materials," J. Mech. Phys. Solids, **41**(2), pp. 389–412.
[18] Anand, L., 1996, "A Constitutive Model for Compressible Elastomeric Solids," Comput. Mech., **18**(5), pp. 339–355.
[19] Schröder, J., and Neff, P., 2003, "Invariant Formulation of Hyperelastic Transverse Isotropy Based on Polyconvex Free Energy Functions," Int. J. Solids Struct., **40**(2), pp. 401–445.
[20] Miehe, C., Hofacker, M., and Welschinger, F., 2010, "A Phase Field Model for Rate-Independent Crack Propagation: Robust Algorithmic Implementation Based on Operator Splits," Comput. Methods Appl. Mech. Eng., **199**(45–48), pp. 2765–2778.
[21] Gaston, D., Newman, C., Hansen, G., and Lebrun, G. D., 2009, "Moose: A Parallel Computational Framework for Coupled Systems of Nonlinear Equations," Nucl. Eng. Des., **239**(10), pp. 1768–1778.
[22] Ayachit, U., 2015, "The Paraview Guide: A Parallel Visualization Application," Kitware, Inc., Clifton Park, NY.
[23] Zhao, X., 2014, "Multi-Scale Multi-Mechanism Design of Tough Hydrogels: Building Dissipation Into Stretchy Networks," Soft Matter, **10**(5), pp. 672–687.
[24] Ducrot, E., Chen, Y., Bulters, M., Sijbesma, R. P., and Creton, C., 2014, "Toughening Elastomers With Sacrificial Bonds and Watching Them Break," Science, **344**(6180), pp. 186–189.
[25] Mao, Y., Lin, S., Zhao, X., and Anand, L., 2017, "A Large Deformation Viscoelastic Model for Double-Network Hydrogels," J. Mech. Phys. Solids, **100**, pp. 103–130.